ACS APPLIED MATERIALS & INTERFACES

RESEARCH ARTICLE

www.acsami.org

End-Group Functionalization of Poly(3-hexylthiophene) as an Efficient Route to Photosensitize Nanocrystalline TiO_2 Films for Photovoltaic Applications

Robin A. Krüger, Terry J. Gordon, Thomas Baumgartner,* and Todd C. Sutherland*

Department of Chemistry, University of Calgary, 2500 University Drive NW, Calgary, AB T2N 1N4, Canada

Supporting Information

ABSTRACT: Bulk heterojunction (BHJ) and dye-sensitized solar cells (DSSCs) have seen increased popularity over recent years and each technology has experienced tremendous improvements in power conversion efficiencies (PCEs), reaching 8 and 12%, respectively. The two technologies have been on independent improvement pathways, and this work establishes a link between them by using the archetypical hole conductor (poly-3-hexylthiophene, P3HT) in BHJs as a sensitizer on TiO_2 for DSSC applications. Three polymers were synthesized and examined as potential TiO_2 sensitizers in DSSCs under AM1.5 solar radiation. Using Grignard metathesis, regioregular P3HT was synthesized then functionalized with either one or two cyanoacrylic acid linker moieties to bind to the TiO_2 surface. End-group modification resulted in minimal changes to the optical and electronic properties as compared to pristine P3HT. Cyclic voltammetry (CV) experiments at anodic potentials of adsorbed sensitizer quantified the amount of alkylthiophene adsorbed on the TiO_2, whereas under reductive sweeps, cyanoacrylic acid end-group binding was determined. CVs of each polymer indicated that loading was drastically different as compared to pristine P3HT with the lowest loading on TiO_2 and monofunctionalized P3HT exhibited the highest loading. The DSSCs showed power conversion efficiencies (PCEs) of 0.1%, 0.2 and 2.2% for the polymer-sensitized TiO_2 of the unfunctionalized, monofunctionalized and difunctionalized polymers, respectively. DSSCs were then subjected to electrochemical impedance spectroscopy (EIS) in the dark and under monochromatic light radiation. The large variance in performance for the functionalized-P3HT sensitizers is attributed to differences in the adsorption modes of sensitizer on the TiO_2 surface, which in the difunctionalized case limits electrolyte recombination and favors forward charge transfer reactions.

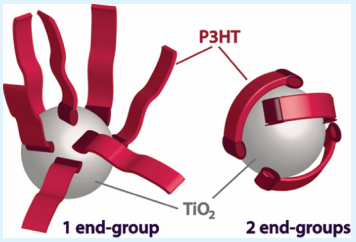

KEYWORDS: energy conversion, polythiophene, thin films, electrochemistry, mesoporous TiO_2, sensitizers

INTRODUCTION

Dye-sensitized solar cells[1] and polymer solar cells[2] have made enormous progress recently and reached the stage of commercial viability, including companies such as, Dyesol, Solaronix, and Peccell Technologies, Inc. Toward solar cell optimization, a plethora of materials have been synthesized, which have provided detailed insight into structure−property relationships such as charge generation and charge transport in a concerted effort to understand and enhance the efficiency of these solar cells. However, improvements in the fields of dye-sensitized solar cells (DSSCs) and polymer-based, bulk-heterojunction (BHJ) solar cells have been carried out independently with little design crossover. The best performing dyes for DSSCs are carboxy-substituted ruthenium polypyridyl complexes that reach efficiencies as high as 12%.[3] Drawbacks of these DSSC materials is the use of rare, expensive metal centers and the synthetic steps needed to prepare the dyes in high purity are often quite extensive. Notable progress has been made by moving away from expensive metals and employ fully organic dyes as inexpensive sensitizers,[4] which has been coupled with lower efficiencies than the ruthenium counterparts and long-term stability. In the BHJ research community, many polymers have been developed for solar cells that have shown very efficient light harvesting properties.[5] Most research has focused on alkylthiophene-derivatives as the donor materials in BHJ solar cells because of its reasonable absorption profile, narrow band gap (~1.9 eV), ability to self-assemble, adopt a favorable phase morphology when blended with an electron acceptor such as [6,6]-phenyl-C61-butyric acid methyl ester (PCBM), high hole mobility (~1 $cm^2\ V^{-1}\ s^{-1}$) and solution processability.[6] Remarkably, there are only a few research groups that have taken advantage of the light harvesting properties and processability of conjugated polymers to sensitize metal-oxides, such as TiO_2.[7] Several strategies are employed to anchor sensitizer molecules to TiO_2, including carboxylic acids, catechols,[8] sulfonates,[9] silanes,[10] and phosphonic acids.[11] Recently, poly(3-hexylthiophene), (P3HT) was synthesized from a silica nanoparticle employing Grignard metathesis (GRIM) of a modified organosilica nanoparticle precursor.[12] To date, two approaches have been explored that merge the properties of conjugated polymers with those of TiO_2 DSSCs. One approach involves the preparation of side-chain functionalized polyelectrolytes with carboxylic acid and cyanoacrylic acid moieties to promote chemisorption of the polymer sensitizer on TiO_2 through alkyl chain or arylamine spacers, which resulted in photovoltaic performances ranging from 0.33 to 3.39%.[7h−l,13] The second approach

Received: March 2, 2011
Accepted: April 27, 2011
Published: May 12, 2011

Scheme 1. Synthesis of Polymers P1−P3

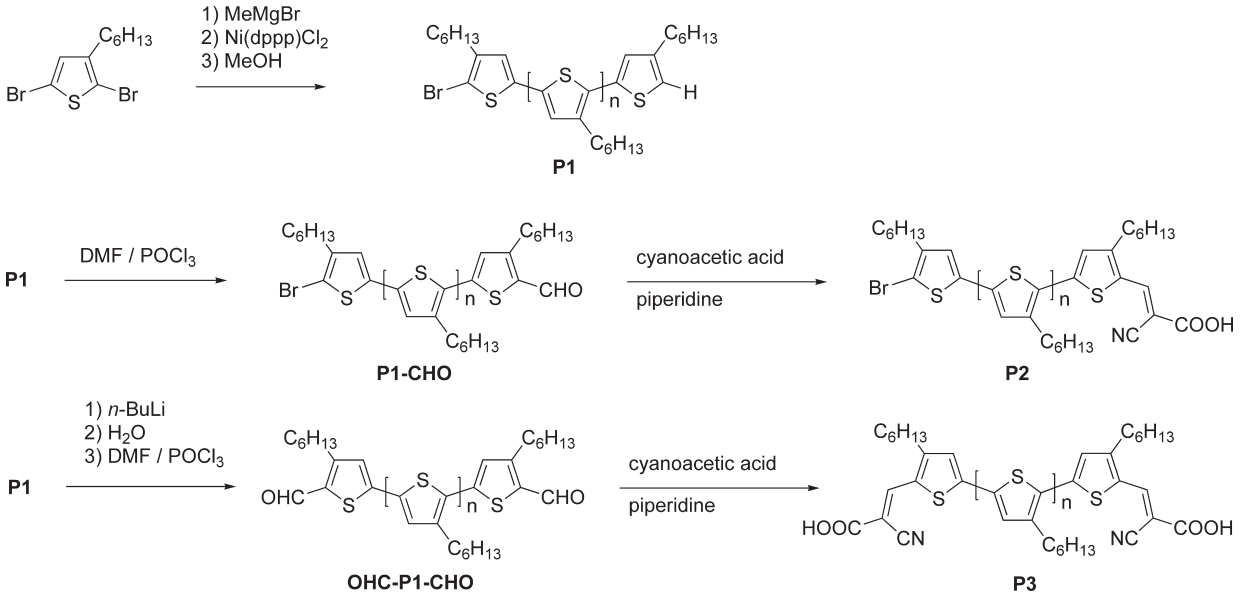

installs carboxylic acid linkers directly to the conjugated polymer backbone, either along the main chain or as end-groups, and exhibited a similar range of PCEs between 0.9 to 2.99%.[7c,d,f,m] Importantly, only one account reports the end-group functionalization of polythiophene for use as a TiO_2 sensitizer for solar cell applications with a photovoltaic performance of 0.9%.[7c]

Here we report on the efficient and facile end-group functionalization of regioregular P3HT that enables chemisorption via cyanoacrylic acid linkers onto mesoporous TiO_2 and illustrates the material's potential as a potent polymer sensitizer for DSSC applications.

RESULTS AND DISCUSSION

Polymer Synthesis and Characterization. The Grignard metathesis (GRIM) polymerization, developed by McCullough[14] to obtain highly regioregular P3HT, **P1**, was employed as depicted in Scheme 1. Because of the proposed reaction mechanism of the GRIM polymerization,[15] the majority of the terminal thiophenes will possess an alpha-hydrogen or an alpha-bromine substituent (H/Br) and a minor fraction of the polymer will be alpha-hydrogen terminated at both termini (H/H).[15a]

Regioregular **P1** was further functionalized with cyanoacrylic acid because this functional group has been shown to bind efficiently to mesoporous TiO_2.[16] End-group functionalization[17] is potentially more advantageous than backbone functionalization because it does not lead to unwanted twisting of the polymer main chain and consequently a decrease in the effective π-conjugation.[18] **P1** was functionalized in a stepwise manner via Vilsmeier−Haack formylation and subsequent Knoevenagel condensation with cyanoacetic acid. Typically, the GRIM polymerization method yields **P1** with different end-groups, which enables the chemical differentiation of the chain ends. Formylation[19] of H/Br terminated **P1** leads to the substitution of the terminal hydrogen with an aldehyde moiety while leaving the bromine on the other polymer terminus, resulting in **P1-CHO** in high yield of 95% (Scheme 1). To install anchoring groups at both ends of **P1** the terminal bromine was removed prior to the formylation by reaction with *n*-butyl lithium and subsequent quenching of the lithiated polymer with water yielding the symmetric H/H terminated polymer that was then formylated to yield **OHC-P1-CHO** in 94% yield. Successful formylations of

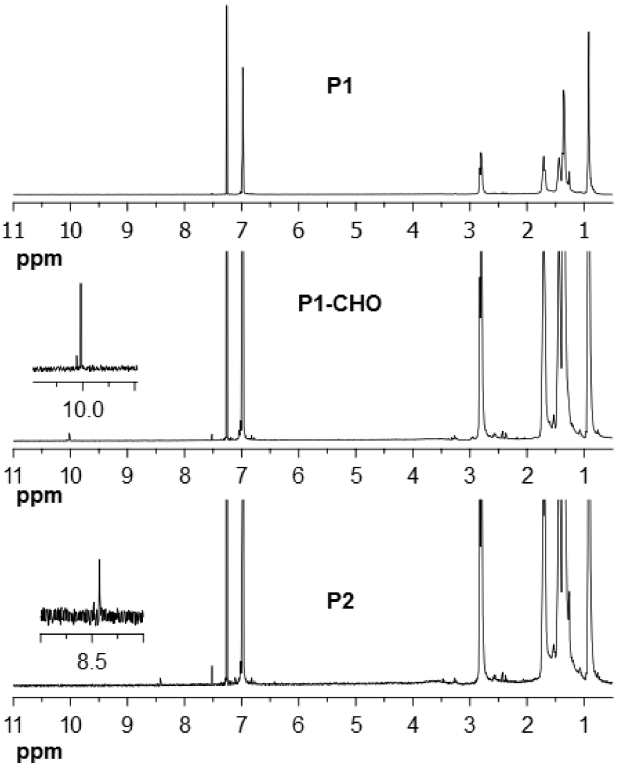

Figure 1. ^{1}H NMR (400 MHz) spectra of **P1**, **P1-CHO**, and **P2** in chloroform. Insets show expansions of resonances of introduced functional end-groups.

Table 1. Physical Properties of P1, P2, and P3

sample	TGA (°C)[a]	DSC T_m/T_c (°C)[b]	M_n (kDa)	M_w (kDa)	PDI
P1	454	221/190	10.5	14.3	1.36
P2	450	217/187	5.4	12.4	2.29
P3	283	[c]	7.2	13.7	1.90

[a] Heating rate of 10 °C/min under nitrogen until weight loss of 5%. [b] Heating rate of 5 °C/min under nitrogen. [c] Not observed before decomposition occurs.

P1 were confirmed by characteristic ^{1}H NMR-spectroscopic changes, shown in Figure 1 and the Supporting Information Figure S1. The aldehyde proton has a resonance at 10.02 ppm and the α-methylene group of the formylated terminal thiophene rings appears as a new triplet at 2.95 ppm. Furthermore, integration of these signals in comparison with the diagnostic signals at 6.98 ppm (β-hydrogen atoms of the thiophene) and 2.81 ppm (α-methylene groups) confirms a quantitative substitution of terminal hydrogen atoms by formyl groups. Note, that both polymers, **P2** and **P3**, have a tendency to aggregate in solution, as assessed by the appearance of three to five additional resonances in ^{1}H NMR at ~10 ppm, which coalesced in diluted NMR samples. Because of the large excess of formylation reagents, it cannot be ruled out that minor amount of β-thiophene was also formylated during the reaction.

Formylated polymers, **P1-CHO** and **OHC-P1-CHO**, were reacted with cyanoacetic acid to give the terminal monocyanoacrylic acid, **P2**, or dicyanoacrylic acid, **P3**, via a Knoevenagel type condensation, as shown in Scheme 1. Partial conversions in the Knoevenagel reaction would result in polymer mixtures that are not easily separated, thus reaction conditions were sought that provide quantitative transformations of the aldehyde moieties by borrowing techniques from small molecule syntheses.[4a] To achieve a quantitative Knoevenagel condensation for **P1-CHO** and **OHC-P1-CHO** the reaction must be performed in refluxing chloroform containing excess base, at least 200-fold excess of the reagents and in the presence of molecular sieves. After an aqueous workup, precipitation from methanol and Soxhlet extraction with methanol and chloroform, quantitative transformation of the aldehyde was confirmed by complete disappearance of the ^{1}H NMR signal at ~10 ppm for both polymers **P2** and **P3**. Furthermore, the appearance of a new resonance at 8.43 ppm is diagnostic for the vinylic proton of the anchoring group (Figure 1). Neither polymer, **P2** nor **P3**, exhibited a ^{1}H NMR distinct resonance for the carboxylic acid, which is not unusual because these signals are usually broad and difficult to observe. Note that **P2** and **P3** also have a tendency to aggregate in solution, as supported by the line broadening in the ^{1}H NMR spectra, especially in the case of **P3** (see the Supporting Information, Figure S1).

Further evidence for the installation of the cyanoacrylic acid end-group on the polymer chains is obtained through IR-spectroscopy (see Supporting Information Figure S2). Drop cast films of **P2** and **P3** on NaCl plates show a characteristic C≡N stretch at 2214 cm^{-1} and C═O stretch at 1683 cm^{-1} that are absent in **P1**. Furthermore, a weak and broad absorption, typical for O−H vibrations, emerges in the IR spectra of **P2** and **P3** between 3200 and 1800 cm^{-1}.

The thermal properties and molecular weights of **P1**−**P3** are summarized in Table 1. Thermogravimetric analysis (TGA) reveals that all polymers **P1**−**P3** are stable up to at least 280 °C under nitrogen (see Figure S3 in the Supporting Information). Differential scanning calorimetry (DSC) thermograms of **P1**and **P2** (see Figure S4 in the Supporting Information) show that introduction of one cyanoacrylic acid group does not have a noticeable influence on the thermal behavior; both **P1** and **P2** exhibit melting points at 220 °C and recrystallize at 190 and 185 °C, respectively. The melting points of **P1** and **P2** show features that appear as a broad endothermic peak with a shoulder at higher temperature, and crystallization of **P1** and **P2** upon cooling is observed as one well-defined exothermic transition. This thermal behavior is reproduced in subsequent cycles and can be attributed to different polymer morphologies. The DSC thermogram for **P3** exhibits different features compared to **P1** and **P2**, as no melting was observed prior to decomposition, implying a small chemical modification of both polymer termini has a significant influence on its thermal properties.

Gel permeation chromatography (GPC) was employed to estimate molecular weights for **P1**, **P2** and **P3**. Due to the monomodal elution profiles observed in GPC traces, a broad distribution of polymer chains with significantly different chain lengths can be ruled out. An intrinsic problem with these experiments is that they can commonly overestimate the molecular weight of rod like polymers, such as **P1**−**P3**, when calibrated with flexible, globular polystyrene. GPC experiments reveal that **P1** contains approximately 60 repeat units with a relatively narrow polydispersity index (PDI) of 1.36. End-group functionalization increases the intrinsic error further due to interactions of **P2** and **P3** with the column stationary phase, resulting in a virtual decrease in molecular weight (i.e., longer elution time) and broadening of the PDI. An important observation is that all elution profiles are still monomodal for **P2** and **P3**, which supports that chain−chain coupling did not occur under the formylation or Knoevenagel reaction conditions.

Physical Properties−Optical and Electrochemical. For solar applications, the effect of end-group modifications on the polymer optical properties is of paramount importance, which is assessed by absorption spectroscopy. Solutions of **P1** in chloroform show features common to P3HT, such as an unstructured absorption profile with an onset at 542 nm and a maximum at 451 nm. Installation of one anchoring group (**P2**) does not affect the absorption properties significantly, as shown in Figure 2a and summarized in Table 2. Conversely, **P3**, with two cyanoacrylic acid moieties, exhibits a broad absorption profile, a red-shifted onset of 15 nm and a 20 nm blue-shifted absorption maximum, as compared to the parent polymer. Spin-coated films of **P1** on glass substrates from chlorobenzene show typical characteristics of solid state P3HT, broad absorptions with an onset at 662 nm and vibronic features. These features are well-known for P3HT and diagnostic for the partial crystallinity of the material in the solid-state caused by $\pi-\pi$ interactions and van der Waals interactions, such as alkyl chain interdigitation. The installation of one cyanoacrylic acid group at the end of the polymer chain of **P2** does not alter the ability of **P2** to form well-organized structures in the solid-state, as supported by the structured absorption profile shown in Figure 2a, which is nearly identical to the absorption profile of **P1** (see Figure S5 in the Supporting Information). In the case of **P3**, with two acid functionalities, the thin film absorption profile is unstructured and possesses a blue-shifted λ_{max} as compared to **P1** and **P2**, suggesting a less-ordered thin film morphology, as illustrated in Figure 2a. It is likely that the two carboxylic acids of **P3** form hydrogen-bonded networks, forcing the polymer chains into a nonplanar

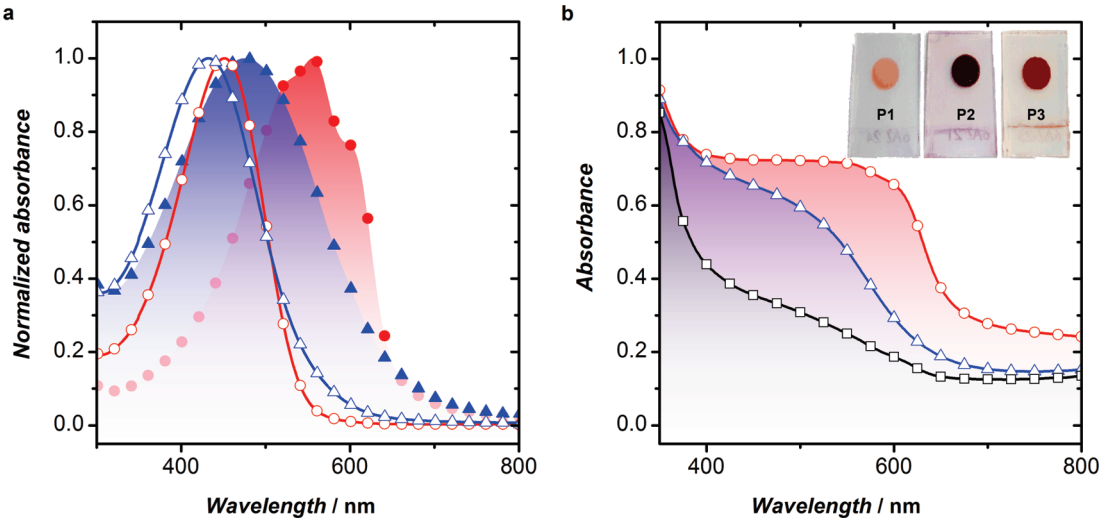

Figure 2. (a) UV−vis absorption spectra of **P2** (circles) and **P3** (triangles) in chloroform solutions (lines) and films on glass (solid fills). (b) UV−vis absorption spectra of **P1** (squares), **P2** (circles), and **P3** (triangles) adsorbed on 6 μm thick TiO_2 films. Inset: photograph of polymers loaded on TiO_2.

Table 2. Optical and Electrochemical Summary of Polymers P1, P2 ,and P3 in Solution ($CHCl_3$) and Thin Films

sample	absorption onset solution (nm) (eV)[a]	absorption onset film (nm) (eV)[b]	E_{OX} vs Fc/Fc^+ (V)[c]	E_{HOMO} (eV)[d]	E_{LUMO} (eV)[e]
P1	542 (2.20)	662 (1.87)	0.46	−5.26	−3.39
P2	535 (2.32)	653 (1.90)	0.35	−5.15	−3.25
P3	557 (2.23)	649 (1.91)	0.29	−5.09	−3.18

[a] In chloroform. [b] Spin-coated from chlorobenzene solutions. [c] Drop-cast from chloroform solution on a glassy carbon working electrode. [d] Assuming the Fc/Fc^+ HOMO energy level at −4.8 eV. [e] E_{LUMO} calculated from the electrochemical oxidation potential onset and the UV−vis absorption onset.

conformation, whereas the single carboxylic acid in **P2** has less ability to hydrogen-bond and is capable of maintaining a planar configuration of the long polymer chains through $\pi-\pi$ and van der Waals interactions. Lohwasser and co-workers[7c] observed similar morphological changes with carboxy-terminated P3HT using P-XRD. The absorption profiles of **P1**, **P2**, and **P3** loaded to TiO_2 is shown in Figure 2b and all exhibit similar absorption onsets to the spin-cast films, extending as far as ∼725 nm for **P2** and **P3**, and ∼650 nm for **P1**. However, the absorption profiles of Figure 2b, show a clear difference in optical density, which is correlated to the loading quantity on TiO_2 and **P2** is more densely packed, followed by **P3** then the control polymer without anchoring group, **P1**. Attempts were made to desorb and quantify the amount of bound polymers by incubating the TiO_2 films in basic EtOH and THF, however, no quantifiable polymer was desorbed by UV−vis absorption assessment, rendering this typical assay for loading quantity not practical for these polymers. Photographs of the polymer solutions can be found in Figure S6 in the Supporting Information and sensitizers adsorbed on TiO_2 are shown as an inset in Figure 2b; and differences in the color of the adsorbed materials can be clearly observed, even though all loading concentrations were similar, which will be discussed in more detail below.

To evaluate the HOMO energy levels of **P1**, **P2** and **P3**, cyclic voltammagrams (CVs) were measured for drop cast films of **P1**−**P3** from chloroform solutions on a glassy carbon working electrode (Figure S7). Although differences in the oxidation potentials are small, ∼0.06 to 0.10 V vs Fc/Fc^+, there is a clear trend to lower oxidation potential as the number of cyanoacrylic acid groups increases from **P1** to **P3**. This trend is likely due to deprotonation of **P2** and **P3** in the electrolyte solution and thus the carboxylate terminated polymers are easier to oxidize. The onsets of the oxidation potentials can be employed to estimate the HOMO energy levels, assuming the Fc/Fc^+ HOMO energy level is located at −4.8 eV.[20] In conjunction with the optical absorption onset of the films, which estimates the HOMO−LUMO energy gap, the LUMO energy levels can also be approximated. Importantly, the overall optical and electronic features of **P1**, **P2**, and **P3** are similar, and thus any differences observed in solar cell performance will be likely due to the cyanoacrylic acid linker chemistry, the TiO_2 surface interactions with the polymer main chains, and polymer−polymer interactions.

The experimentally determined E_{LUMO} levels of polymers **P1**−**P3** indicated that the energetics are thermodynamically favorable to inject electrons into the TiO_2 conduction band. Likewise, the E_{HOMO} level is lower in energy than the I^-/I_3^- redox couple in the electrolyte solution, which is needed for regeneration of the photo-oxidized sensitizer.

The TiO_2 was incubated in a solution containing ∼6 mg of polymer in 10 mL of chloroform for 18 h at room temperature in the dark. Excess loosely bound polymer was rinsed from the TiO_2 surface with THF until the rinsing solvent was colorless. Polymer sensitizer-loaded TiO_2 working electrodes were then subjected to CV analysis to determine the amount of thiophene and cyanoacrylic acid that were electrochemically accessible by changing the electrode potential. The oxidative scans of **P1**, **P2**, and **P3** to assess the quantity of thiophenes that are electrochemically oxidizable on the electrode are shown in Figure 3. There are two characteristics in describing TiO_2 films of **P1** to

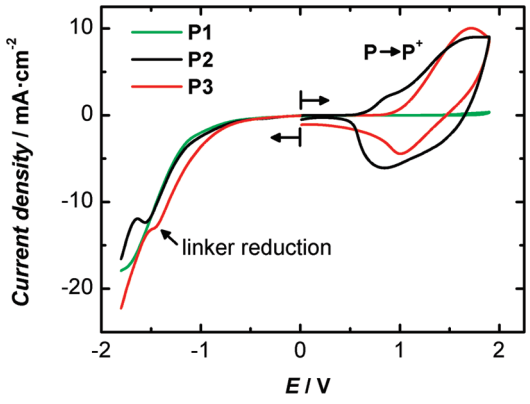

Figure 3. Oxidative and reductive potential sweeps of adsorbed **P1**, **P2**, and **P3** on 6 μm thick TiO_2 on FTO. Scan rate: 500 mV s^{-1}.

P3: First, the oxidation current due to the oxidation of thiophene rings, and second, the capacitance of the films on the TiO_2 substrates. **P1** shows little oxidation current (integrated charge of 8.1 μC) due to electrochemically oxidizing **P1** up to 1.7 V (vs Ag|AgCl|CH_3CN), suggesting the loading is very low and the **P1** that is bound has minimal contact with the substrate, which is corroborated by the lighter color film for **P1** on TiO_2, shown in Figure 2b inset. The capacitance of the **P1** film is 4.5 μF cm^{-2} at 0.4 V, where no faradaic current is produced. **P2** sensitized TiO_2 shows a much larger oxidizing current in the thiophene oxidation region and integrates to 3.4 mC, indicating a much larger loading compared to **P1**, which is consistent with the observed color of the loaded dye as shown in Figure 2b inset. Note the capacitance of the TiO_2 film adsorbed with **P2** has increased to 100 μF cm^{-2} at 0.4 V, suggesting the film/sensitizer has a higher dielectric constant than **P1**, which is consistent with an oxidized (electrochemically p-doped) film and counterion flux. **P3** also shows electrochemical oxidation peaks due to thiophene and the total charge is similar to **P2** at 3.3 mC, indicating a similar quantity of oxidizable thiophenes are present on the TiO_2 substrate. Interestingly, the film capacitance measured at the same potential (0.4 V) increases to 339 μF cm^{-2}. Assuming electrode areas are the same, capacitance values are proportional to permittivity of the film and inversely proportional to film thickness of the sensitizer layer. The capacitance values suggest **P1** is a thin film that is highly penetrated with electrolyte, **P2** is a thicker film that is moderately oxidatively doped and **P3** forms a similar thickness layer to **P2** and a film that is heavily oxidatively doped. Note, **P2** also exhibits a small shoulder at <1 V, which could be due to different microenvironments of this loaded polymer on TiO_2 because this shoulder is absent in the drop cast films on a glassy carbon electrode. In a separate experiment, the polymer films on TiO_2 were subjected to a reductive potential sweep, as shown in Figure 3, which should electrochemically reduce the linker group. The reductive potential sweep for **P1** does not display a reduction peak, as expected because it does not contain the cyanoacrylic acid linker. Both **P2** and **P3** do show reduction peaks and the resulting integrated current for **P2** and **P3** is 0.44 mC and 0.26 mC, respectively. Surprisingly, the total charge of the reduction peak for **P2** is nearly double that of **P3**. Normalizing the integrated current by dividing by the number of redox active cyanoacrylic acid moieties, suggests that the number of polymer chains attached to the TiO_2 surface for the **P2** film is approximately four times that of the **P3** sensitized film. However, the oxidation peaks of thiophene show similar quantities of polythiophene are electrochemically oxidizable. The difference in linker loading suggests that the **P3** sensitizer has more redox-active thiophenes, which could be due to a higher p-doping ability of **P3** compared to **P2**. On the basis of the quantity of cyanoacrylic acid linker present, the **P2** sensitizer likely exists as a close-packed monolayer extending outward toward the electrolyte, whereas **P3** possessing two binding moieties, orientates itself in a more flat/planar configuration along the TiO_2 surface. With both the quantity of thiophene in contact with the electrode and the number of cyanoacrylic acid groups, a model of the polymer film can be constructed and is shown in Figure 4.

Taking into account the optical and electrochemical data permits the formation of a model to explain the differences in the film properties, shown in Figure 4. The TiO_2 particles are approximately 20 nm in diameter and the outstretched polymers would be of similar dimension as illustrated by the mesoporous TiO_2 supported on FTO. In the case of **P1**, the polymer chains physisorb to the TiO_2 surface at low loading, as supported by both optical and electrochemical measurements and the electrolyte has ready access to the TiO_2 surface. In **P2** devices, the polymer chemisorbs to the TiO_2 surface at much higher density than **P1**, as supported by optical measurements and CV sweeps. **P2** shows a much higher number of cyanoacrylic acid groups bound to the TiO_2, but the amount of thiophene that is in electrochemical contact with the electroactive surface is only moderate. The **P2** film is modestly oxidatively doped and the density of polymer chains may result in the chains 'standing' on end. The higher loading of **P2** sensitized TiO_2 is supported by the optical density of the devices shown in the inset of Figure 2b. The difference in loading density is partly responsible for the difference in the observed open circuit voltage (V_{OC}), see below, due to a greater surface acid concentration leading to protonated TiO_2.[7f] In the case of **P3** devices, the number of linker groups attached to the TiO_2 is less than **P2**, but the amount of redox active thiophene is the same, suggesting intimate contact of the thiophene rings with the TiO_2 surface leading to a much higher p-doping level than **P2**. If the double-linker **P3** sensitizer is lying flat on the surface, then the electron-rich heterocycles may increase the conduction band of TiO_2 leading to a larger V_{OC} as will be discussed in the following section.

Device Fabrication. With the knowledge that **P2** and **P3** adsorb to TiO_2 via the cyanoacrylic acid linker, polymer-sensitized solar cells were fabricated and the current density–voltage (*JV*) characteristics were measured under AM1.5 irradiation at 100 mW·cm^{-2}. Components for cell fabrication, namely the thickness of the TiO_2 substrates (6 μm) and choice of electrolyte (Dysesol High Performance Electrolyte (HPE)) were chosen for the following reasons. Thinner TiO_2 films were employed because the polymer sensitizers strongly absorb between 400 and 650 nm and because of the anticipated high sensitizer loading due to the cyanoacrylic acid linker, which is known to possess excellent TiO_2 binding characteristics, and the molecular weights of polymers employed (>12 kDa). The electrolyte, which is a critical component in Ru-based and fully organic devices, was selected because it has been shown to perform well in Ru-based DSSC applications under the testing conditions. The *JV* performance curves for **P1** through **P3** are shown in Figure 5. Dramatic differences in both the short circuit current (J_{SC}) and open circuit voltage (V_{OC}) are apparent between **P1**, **P2**, and **P3**. The J_{SC} measured for the polymer devices **P1**, **P2** and **P3** were 0.41, 0.92, and 6.9 mA cm^{-2}, respectively, which represent nearly an order of

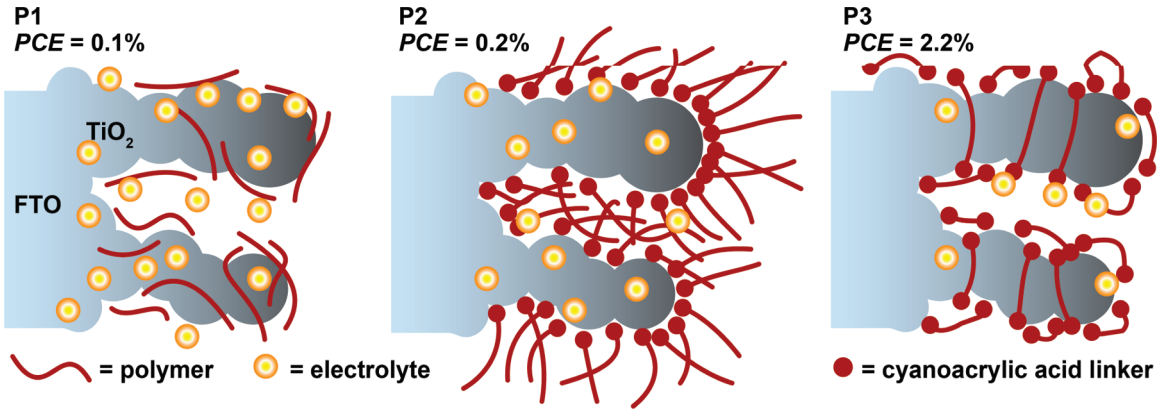

Figure 4. Model of loading of **P1**−**P3** on TiO_2.

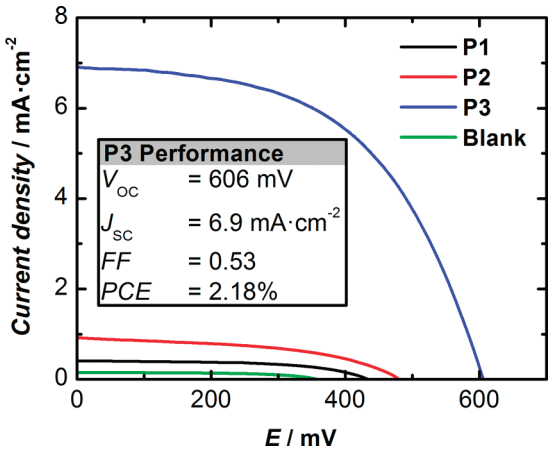

Figure 5. Current density−voltage curves for **P1**, **P2**, and **P3** under AM1.5 irradiation at 100 mW cm^{-2}. Active area: 0.28 cm^2.

magnitude improvement when comparing **P1** and **P2** to **P3**. The breadth of short circuit current densities is likely due to the differences between the polymers' ability to conduct charges and inject electrons to the TiO_2. For example, **P1** exhibits a low current density because (1) only minor quantities of polymer remained on the surface after rinsing and (2) there is no electron-accepting binding motif to facilitate/encourage electron injection into the TiO_2 conduction band upon photoexcitation. On the other hand, **P2** successfully adsorbs to TiO_2, according to the UV−vis and capacitance measurements, but due to its one binding moiety and rigid planar structure, aggregation likely quenches or traps photoexcited states leading to a low current density.[1a] Lastly, **P3** which possesses two cyanoacrylic acid binding groups, forms a sensitizing polymer layer surrounding the TiO_2 without undergoing a detrimental packing of polymer main chains. The observed fill factor (FF) was average, ranging from 0.47 to 0.56 for all three polymers, which is comparable to other reports for an end-group functionalized polymer sensitizer.[7c] The open circuit voltage (V_{OC}) for **P1** and **P2** was reasonable at 434 mV and 481 mV, respectively, but remarkably high for **P3** at 606 mV. The large variance observed in V_{OC} for **P1**−**P3** will be discussed below. Thus, the resulting power conversion efficiency of devices containing **P1**, **P2**, and **P3** were 0.1, 0.2, and 2.2%, respectively. The PCE observed for **P1** is comparable to that recently reported by Satapathi and co-workers.[21] The PCE for **P3** is of the same order of magnitude as current state-of-the-art systems, for example for backbone functionalized polymer sensitizers at 2.99%[7d] and 3.39%[7l] and 0.9%[7c] for end-group functionalized materials. To the best of our knowledge, the PCE value obtained for **P3** represents the highest reported for an end-group functionalized polymer sensitizer in a DSSC application.

As shown in Figure 5, the V_{OC} is improved when employing a sensitizer with two binding moieties, **P3**, as compared to the monofunctionalized sensitizer, **P2**, and unfunctionalized **P1**. Because sensitizers **P1** to **P3** are very similar in structure, except for the incorporation of the cyanoacrylic acid linker, it may be surprising that the V_{OC} is so markedly different. Two factors combine that may explain the differences in the observed V_{OC} − polymer loading quantity and the TiO_2 conduction band. Using the CV-derived capacitance measurements as discussed above, the V_{OC} appears dependent on concentration of holes and counterions in the polymer backbone on the FTO/TiO_2 surface. **P3** blocks the surface by forcing the thiophenes to lie down and restrict access of the electrolyte to the TiO_2. As shown by CV experiments, the absolute number of cyanoacrylic acid groups that are bound to TiO_2 is greater in **P2** than **P3** and results in a decrease in the work function of TiO_2 due to "acid-doping" of the TiO_2 surface yielding a larger observed *Voc*.[7f] Furthermore, **P3**, which has a higher electrochemically determined p-doping level than **P1** or **P2**, could change the TiO_2 conduction band resulting in a lower V_{OC}. The lower V_{OC} observed in **P1** can be attributed to electrolyte access to the TiO_2 surface because a similar V_{OC} was observed for a cell containing no sensitizer (~0.4 V), shown as the blank in Figure 5. Since **P1** shows such lower capacitance, it implies the electrolyte has direct contact with the electrode and V_{OC} resembles an electrolyte only control cell. **P2** shows better electrolyte blocking behavior and higher oxidatively doped polymer than **P1**, as assessed by the capacitance value but the increased number of anchor groups may cause an acid-doped TiO_2 surface, which has been documented to lower the V_{OC}.[7f]

To better understand the wide variance in the photovoltaic performance of **P1**, **P2**, and **P3**, we employed electrochemical impedance spectroscopy (EIS) to gain insight into the interfacial dynamics under dark conditions and under monochromatic illumination at 455 and 610 nm. The resulting Nyquist and Bode plots are shown in Figure 6. While in the dark, devices held under applied forward bias (at V_{OC}) yield information about injected conducting band electrons within the TiO_2 particles as well as their movement as it is coupled to the iodide ions (I^-/I_3^-) in the electrolyte. In the dark, DSSCs were held at V_{OC} and an impedance spectrum from 300 kHz to 1 Hz was collected with a 10 mV *ac* excitation amplitude. Both **P1** (see Figure S8 in the

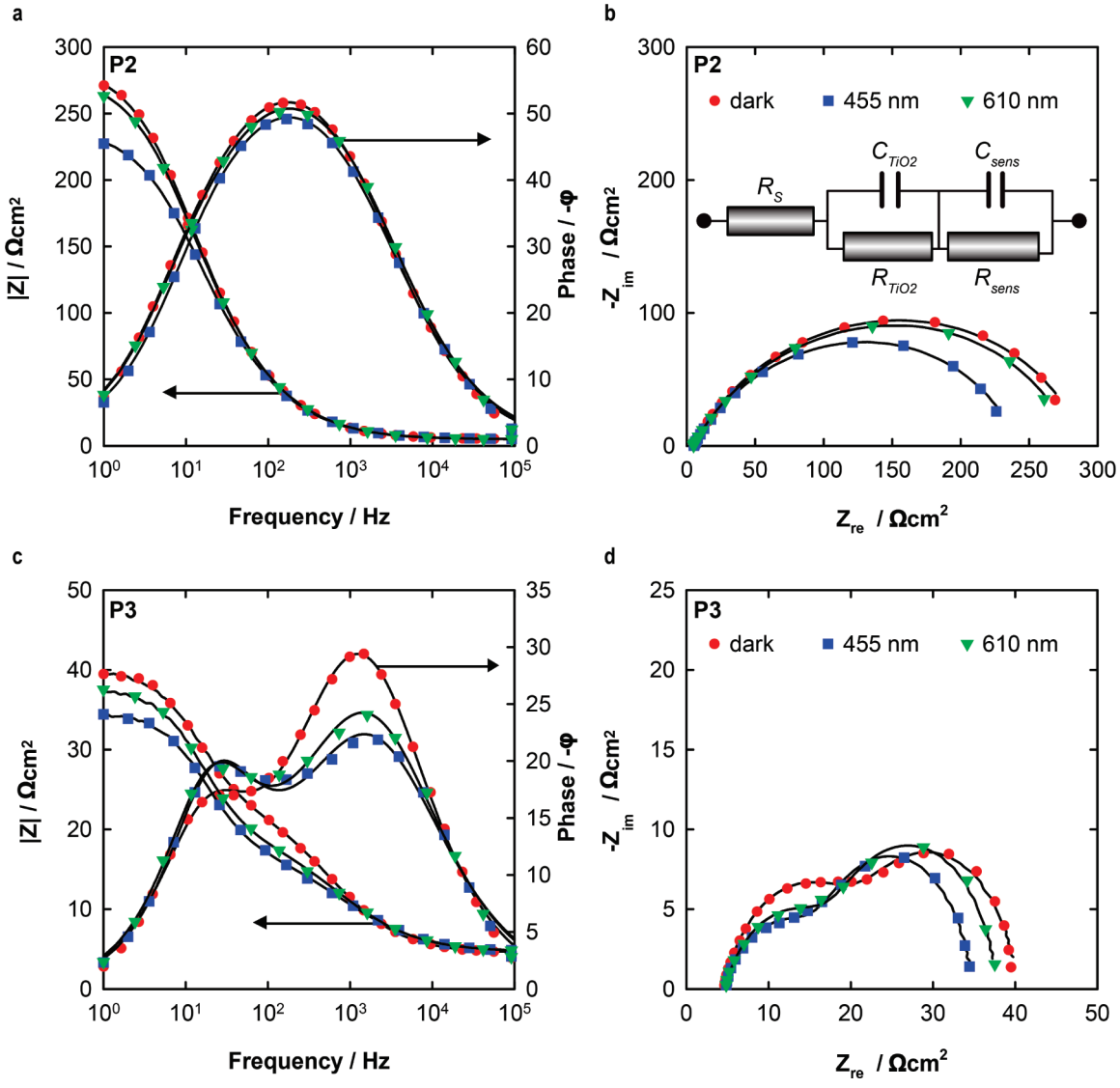

Figure 6. (a) Bode plot and (b) Nyquist plot of **P2** in the dark (circles) and under monochromatic illumination (squares −455 nm, 100 mW cm^{-2} and triangles −610 nm, 30 mW cm^{-2}). (b) Inset: equivalent circuit used to fit all EIS data. c) Bode plot and d) Nyquist plot of **P3** in the dark (circles) and under monochromatic illumination (squares −455 nm, 100 mW cm^{-2} and triangles −610 nm, 30 mW cm^{-2}). All raw data are shown as points and the best fits to the equivalent circuit are shown as black lines.

Supporting Information) and **P2** show nearly superimposable impedance spectra, thus only **P2** and **P3** device EIS plots are shown. The Nyquist plots of **P2** and **P3** (Figure 6b and 6d), at V_{OC} in the dark, show very different behavior. In the **P2** case, the Nyquist plot (Figure 6b) displays a single semicircle with diameter of approximately 275 Ω·cm^2, which would be consistent with a simple *RC* circuit and a single time constant; however, the Bode phase plot (Figure 6a) is very broad and suggests a small hidden peak could be present at higher frequencies. Conversely, **P3** devices show two semicircles in the Nyquist plots (Figure 6d), diagnostic of two time constants and the diameters of each semicircle are an order of magnitude smaller in resistance than the **P2** devices. Given that the sensitizers are similar in structure, the same equivalent circuit model, shown as an inset of Figure 6b, was chosen to fit the data. The chosen circuit consists of two *RC* circuits in parallel to represent the two time constants and a resistor in series to represent the conductivity of the FTO, electrolyte and Pt counter electrode. Note that constant phase elements (CPEs) were used in all fits and because the exponential modifiers (α) are approaching unity, the CPEs are treated as capacitors.

A variety of equivalent circuits that are used to fit impedance data of DSSCs were initially chosen to fit the data in Figure 6. However, most equivalent circuit models used in DSSCs did not result in satisfactory fitting. Using the standard DSSC impedance fitting circuits, led to fitting that was over parametrized, and certain circuit elements were not needed. The minimalist circuit chosen, as shown in Figure 6b, resulted in fit errors of approximately 1% and importantly, every circuit element has significance in the overall fitting process. A summary of all impedance data curve fitting is included in Table 3.

The only difference between all photovoltaic cells tested is the polymer sensitizer coating the TiO_2, thus each cell should and does show similar resistance terms for solution resistance, R_s, which includes the FTO resistance, at ∼6 Ω cm^2. The first RC circuit, which represents fast reactions occurring at the

Table 3. Summary of EIS Data Obtained for P1, P2, and P3 under Dark and Illuminated Conditions at Open Circuit[a]

sample	R_S (Ω cm^2)	C_{TiO_2} (μF cm^{-2})	α_{TiO_2}	R_{TiO_2} (Ω cm^2)	C_{sens} (μF cm^{-2})	α_{sens}	R_{sens} (Ω cm^2)
P1 dark	5.9	29.6	0.77	239	114	0.99	127
P1 455 nm	5.0	27.9	0.78	213	129	1.00	133
P1 610 nm	5.9	28.6	0.77	252	114	0.99	134
P2 dark	5.0	18.2	0.70	171	82	0.82	118
P2 455 nm	5.0	18.2	0.67	147	75	0.82	95
P2 610 nm	5.0	17.5	0.69	169	79	0.82	113
P3 dark	4.5	16.1	0.75	17	343	0.85	19
P3 455 nm	4.8	16.1	0.71	10	218	0.81	20
P3 610 nm	4.8	16.1	0.72	12	229	0.82	22

[a] α is the exponential modifier of the CPE in the employed EIS model.

FTO/TiO_2/Polymer interface at high frequency, includes C_{TiO_2} and R_{TiO_2} in Table 3. Across the series of sensitizers studied, the capacitance of the first interface does not change significantly, as expected since all devices were prepared using the same FTO and TiO_2. The capacitance of the first interface varies from 14 μF cm^{-2} for **P3** to 29 μF cm^{-2} for **P1**, suggesting a similar interface exists in each device. Also note that the alpha-values in the CPEs range between 0.7 and 0.8, which suggests a porous electrode and is consistent with the notion of the mesoporous TiO_2 layer. The resistance terms (R_{TiO_2}) are similar for **P1** and **P2** at 220 and 170 Ω cm^2, respectively, and **P3** is much more conductive with R_{TiO_2} at 18 Ω cm^2 in the dark. This large difference in resistance to electron movement suggests a barrier to shuttling electrons to and from the polymer|TiO_2 interface in **P1** and **P2**, which is absent in **P3**. Clearly, the addition of the double linker approach to polymer-sensitized DSSCs has advantages at the TiO_2 interface. Under monochromatic light (either 455 nm or 610 nm) at V_{OC}, the C_{TiO_2} terms remain similar to the dark capacitance, suggesting no permittivity or TiO_2 interface change with light exposure. Interestingly, the resistance term, R_{TiO2}, decreases upon exposure to 455 nm light and remains the same in the dark and under 610 nm light exposure, suggesting the 455 nm light causes some direct excitation of the TiO_2 leading to higher conductivity within the semiconductor for the three sensitizers. Direct excitation of the TiO_2 interface is feasible, based on the absorption profile of the sensitizer loaded on the TiO_2, as shown in Figure 2b.

The second RC circuit, consisting of C_{sens} and R_{sens}, represents the polymer sensitizer on the TiO_2 and is correlated to the inherent charge transport properties of the polymer sensitizers and dye regeneration reactions. In the dark, under V_{OC} conditions, the capacitance values correlate with the CV-determined capacitance values with **P3** representing a more oxidatively doped film with a higher capacitance at 340 μF cm^{-2} compared to **P1** or **P2** at ~110 μF cm^{-2}. Upon exposure to light, we expect the creation of holes, which would in turn require counterions to infiltrate the polymer leading to a lower capacitance due to the change in permittivity. While **P3** does show a large decrease in capacitance upon irradiation with 455 nm light and a small change with 610 nm, relative to the dark capacitance, which is consistent with creating holes in the P3HT main chain, both **P1** and **P2** do not show a capacitance change upon irradiation. Since the absorption profiles of **P1** to **P3** on TiO_2 show bands at 455 and 610 nm, radiation should result in excited states, however, in the **P1** and **P2** devices these excited states are not successful at injecting their electrons in the TiO_2, to generate the holes. This effect could be due to low loading levels for **P1** case and aggregate quenching excited states for the **P2** case.[22] The resistance terms (R_{sens}) for sensitizers **P1** to **P3** are a measure of the conductivity of the polymer layers. In the dark under V_{OC} conditions, the resistance of the sensitizer films of **P1** and **P2** is rather high at 120 and 130 Ω cm^2, respectively, compared to sensitizer **P3** at 20 Ω cm^2. These resistance terms (R_{sens}) indicate the P3HT main chain is not sufficiently doped at V_{OC} in the dark and may explain the lower performance of these cells containing **P1** and **P2**. Assuming the rate determining step in the generation of current in the polymer-sensitized solar cell is the charge transport within the polymer film, then the higher conductivity of **P3** explains the larger current density observed in the *JV* performance curve.

CONCLUSIONS

Dye-sensitized solar cells have been fabricated using end-group functionalized P3HT. Simple Vilsmeier−Haack formylation and subsequent Knoevenagel condensation reactions were employed to quantitatively install cyanoacrylic acid binding moieties at the terminal positions of regioregular P3HT. Device performance was heavily dependent on the number of cyanoacetic binding groups. Pristine P3HT was found to fractionally sensitize TiO_2 whereas mono- and difunctionalized P3HT was found to adsorb readily to the TiO_2 nanoparticles. Polymer sensitizers with two binding groups exhibited a PCE of 2.2% whereas polymers with one cyanoacrylic acid binding group exhibited a PCE of only 0.2%. The poor performance of the monofunctionalized sensitizer was likely due to high loading, which lead to polymer aggregation and quenching of the photoexcited states and was reflected in the low short circuit density. The high performance of **P3** is caused by the close contact of the polymer chains with the TiO_2 surface leading to efficient charge injection with minimal opportunity for quenching. These observations are supported by the UV−vis absorption and electrochemical measurements of polymer adsorbed to TiO_2 working electrodes. This ground-breaking report on P3HT sensitizers functionalized with either one or two cyanoacrylic acid binding groups represents a significant step toward merging the favorable properties of both the DSSC and BHJ research communities in the quest for improved solar cell performance.

EXPERIMENTAL SECTION

Reactions were carried out in dry glassware and under inert atmosphere of purified nitrogen using Schlenk techniques. Solvents were dried over appropriate drying agents and then distilled. All reagents were purchased from commercial sources and used as received, unless stated

otherwise. Adapted from Rieke and co-workers 2,5-dibromo-3-hexyl-thiophene was prepared by using NBS as the brominating reagent.[23]

^{1}H NMR spectra were recorded on Bruker Avance-II 400 MHz spectrometers. Chemical shifts were referenced to tetramethylsilane (TMS). Photophysical data were recorded in either chloroform solution or as thin films (spin-coated onto glass substrates) on an UV−vis−NIR Cary 5000 spectrophotometer. Gel permeation chromatography (GPC) analyses were carried out on a Waters Breeze instrument equipped with two styragel HR4E and HR5 columns. Tetrahydrofuran (THF) solutions for GPC analysis were eluted at 30 °C and at a flow rate of 1.0 mL min^{-1} and analyzed using a UV detector. Molecular weights and molecular weight distributions were reported against polystyrene standards. Gel permeation chromatography experiments overestimate the molecular weight of rod like polymers like P3HT[24] when calibrated with polystyrene. Adding polar groups to the polymer chains slows the elution time due to interaction of the polymers with the column material and leads to underestimate the polymer weight. To estimate the yields of the polymers we assumed that the molecular weight of **P1**, determined by GPC, was the highest precision of all polymers studied here. Furthermore, we assumed that end-group functionalization does not affect the molecular weight. Thus, the number average molecular mass (M_n) of **P1** was used to determine the yields of all transformations, even though GPC values of all polymers were available. Thermal analyses were performed using TA-Q200 DSC and TA-Q50 TGA instruments under N_2 atmosphere.

Films were prepared by spin-coating polymer solutions 5−7 mg mL^{-1} in $CHCl_3$ or chlorobenzene (Laurel Technologies, WS-400 × 10^{-6} NPP-lite) under atmospheric conditions using the following conditions: cleaned glass slide (4 cm^2 optical measurements) at 750 rpm for 1 min. Films for cyclic voltammetry measurements were drop cast (5−7 mg mL^{-1} in $CHCl_3$) onto a glassy carbon electrode and air-dried. Cyclic voltammetry was carried out using an Autolab PGSTAT302 instrument, with a glassy carbon disk as working electrode, Pt wire as counter electrode, and a Ag|AgCl|$(n$Bu$)_4$NCl$_{0.1M}$ reference electrode; supporting electrolyte was 0.1 M [NBu$_4$]PF$_6$ in CH_3CN; standard scan rates were 500 mV s^{-1}. Electrochemical impedance spectroscopy (EIS) was performed using a Zahner IM6 impedance analyzer coupled to monochromatic diode light source over a frequency range of 1 Hz to 300 kHz with an *ac* amplitude of 10 mV. Cells were held at their respective open circuit potentials obtained from the *JV* measurements, while the EIS spectrum was recorded. The resulting spectra were fit to an equivalent circuit model using a Thales 4.02 software package.

Device Fabrication. Prescreen printed TiO_2 working electrodes on tec 8 FTO glass were purchased from Dyesol and heated to 500 °C prior to dipping into sensitizing solutions. The films of transparent Dyesol 18NR-T TiO_2 were 6 μm thick and possess an active area of 0.28 cm^2. Polymer sensitizing solutions were prepared by dissolving ∼6 mg of **P1** − **P3** in 10 mL chloroform. The working electrodes were taken out of the oven and dipped into the sensitizing baths while warm; approximately 40−50 °C, sealed and incubated in the dark for 18 h. Following incubation in the sensitizer solution, the films were rinsed with either toluene or THF to remove weakly bound polymer. Films were rinsed until the rinsing solvent was colorless. Working electrodes and predrilled platinized counter electrodes (Dyesol) were heat-sealed together using 30 μm thick thermoplacstic Surlyn gaskets (Dyesol) and a Dyesol Test Cell Assembly Machine sealer. The cells were filled with an acetonitrile-based electrolyte (Dyesol High Performance Electrolyte batch TEL-294F) via a home-built vacuum backing filling apparatus. Finally, cells were then sealed with aluminum-backed thermoplastic sealant using a Dyesol Fill Hole Sealer. Photovoltaic measurements were made using a class A Newport solar simulator with a 150 W Xe lamp and power output was calibrated to an NREL certified monocrystalline Si reference cell. *JV* characteristics were obtained using a Keithley 2420 source meter employing a delay time of 50 ms prior to recording an *JV* curve.

Synthesis. *P1*. According to a method reported by McCullough[14] methylmagnesium bromide in butyl ether (34 mL; 1M) was added to a solution of 2,5-dibromo-3-hexyl-thiophene (11.02 g ; 33.80 mmol) in THF (250 mL) and refluxed for 50 min under an atmosphere of nitrogen. After cooling the reaction mixture to room temperature 1,3-bis(diphenylphosphino)propane nickel(II) chloride (196 mg ; 0.36 mmol) was added in one portion and refluxing was continued for 100 min. Subsequently, the reaction mixture was concentrated to 100 mL and dropped in to methanol (800 mL) under vigorous stirring. The precipitate was collected by filtration and washed with methanol. To remove residual catalyst and short polymer chains, the crude polymer was exhaustively Soxhlet-extracted with methanol and hexanes, respectively. The product was obtained by subsequent extraction with chloroform and precipitation into methanol.

Yield: 2.88 g (50%). M_n = 10.5 kDa, M_w = 14.3 kDa, polydispersity index (PDI) = 1.36. ^{1}H NMR (400 MHz, $CDCl_3$): δ = 6.98 (50H, s, H$_{ar}$), 6.90 (1H, s, H$_{ar}$ of hydrogen terminated end-group), 2.81 (100H, t, α-CH$_2$), 2.62 (2H, t, α-CH$_2$ of hydrogen terminated end-group), 1.76−1.63 (100H, m, β-CH$_2$), 1.50−1.24 (300H, m, CH$_2$), 0.96−0.85 (150H, m, CH$_3$).

P1-CHO. Adapted from Surin and co-workers.[19] A solution of **P1** (490 mg) in dry toluene was deoxygenated by purging with nitrogen for 30 min. DMF (2 mL) and $POCl_3$ (2 mL) were then added. The reaction mixture was stirred at 75 °C under nitrogen in the dark for 24 h before it was cooled to room temperature, quenched with a saturated aqueous solution of sodium acetate (5 mL) and poured into cold methanol (200 mL). The precipitate was collected by filtration and Soxhlet-extracted with methanol for 16 h and then with chloroform. The chloroform fraction was evaporated to dryness and yielded the product as black solid with a green tint.

Yield: 0.47 g (95%). M_n = 10.7 kDa, M_w = 16.2 kDa, polydispersity index (*PDI*) = 1.51. ^{1}H NMR (400 MHz, $CDCl_3$): δ = 10.02 (1H, s, CHO), 6.98 (120H, s, H$_{ar}$), 2.95 (2H, t, α-CH$_2$ of aldehyde terminated end-group), 2.81 (240H, t, α-CH$_2$), 1.77−1.64 (240H, m, β-CH$_2$), 1.50−1.26 (720H, m, CH$_2$), 0.96−0.84 (360H, m, CH$_3$).

P2. Under nitrogen, **P1-CHO** (470 mg), cyanoacetic acid (1 g; 11.7 mmol), and piperidine (1 mL; 10.0 mmol) were dissolved in chloroform (150 mL) and refluxed for 24 h. The condensing chloroform was passed through molecular sieves to bind water that was released by the reaction. The reaction mixture was then poured into diluted HCl (pH ∼3−4). After phase separation, the aqueous layer was extracted with chloroform once. The combined chloroform layers were washed with water (3 × 100 mL), dried with sodium sulfate, and evaporated to dryness. The residue was redissolved in a minimum amount of hot toluene and precipitated into methanol (300 mL methanol containing 1 mL concentrated HCl). The precipitate was collected by filtration and Soxhlet-extracted with methanol for 16 h to remove residual reagents and subsequently with chloroform. The chloroform fraction was evaporated to dryness, redissolved in a minimum amount hot toluene and precipitated into methanol (150 mL of methanol containing 0.5 mL of concentrated HCl). After drying under vacuum the product was obtained as a dark olive green solid.

Yield: 0.45 g (96%). M_n = 5.4 kDa, M_w = 12.4 kDa, polydispersity index (*PDI*) = 2.29. ^{1}H NMR (400 MHz, $CDCl_3$): δ = 8.43 (1H, s, H$_{vinyl}$), 6.98 (82H, s, H$_{ar}$), 2.81 (180H, t, α-CH$_2$), 1.77−1.65 (180H, m, β-CH$_2$), 1.49−1.27 (540H, m, CH$_2$), 0.95−0.84 (270H, m, CH$_3$).

CHO-P1-CHO. Adapted from Surin and co-workers.[19] Under nitrogen, **P1** (500 mg) was dissolved in dry THF (150 mL) and cooled to 0 °C. A solution of *n*-butyllithium in hexanes (4 mL; 2.5M) was then added and the reaction mixture was stirred for 30 min at that temperature before water was added to quench the reaction. The resulting suspension was evaporated to dryness, redissolved in chloroform, washed with water (3 × 100 mL), dried with sodium sulfate, and evaporated to dryness. The remaining residue was

dissolved in dry toluene (80 mL) under nitrogen and DMF (2 mL) and $POCl_3$ (2 mL) were added. The reaction mixture was stirred at 75 °C under nitrogen in the dark for 24 h before it was cooled to room temperature, quenched with a saturated aqueous solution of sodium acetate (10 mL), and poured in to cold methanol (200 mL). The precipitate was collected by filtration and Soxhlet-extracted with methanol for 16 h and then with chloroform. The chloroform fraction was evaporated to dryness and yielded the product as black solid with a green tint.

Yield: 0.47 g (94%). M_n = 8.2 kDa, M_w = 14.5 kDa, polydispersity index (*PDI*) = 1.77. ^{1}H NMR (400 MHz, $CDCl_3$): δ = 10.02 (2H, s, CHO), 6.98 (40H, s, H_{ar}), 2.95 (4H, t, α-CH_2 of aldehyde terminated end-group), 2.81 (80H, t, α-CH_2), 1.77−1.64 (80H, m, β-CH_2), 1.50−1.26 (240H, m, CH_2), 0.96−0.84 (120H, m, CH_3).

P3. Under nitrogen, **OHC-P1-CHO** (100 mg), cyanoacetic acid (0.5 g ; 5.8 mmol) and piperidine (0.5 mL ; 5.0 mmol) were dissolved in chloroform (50 mL) and refluxed for 24 h. The condensing chloroform was passed through molecular sieves to bind water that was released by the reaction. The reaction mixture was then poured into diluted HCl (pH ∼3−4). After phase separation, the aqueous layer was extracted with chloroform once. The combined chloroform layers were washed with water (3 × 100 mL), dried with sodium sulfate, and evaporated to dryness. The residue was redissolved in a minimum amount of hot toluene and precipitated in methanol (200 mL of methanol and 1 mL of concentrated HCl). The precipitate was collected by filtration and Soxhlet-extracted with methanol for 16 h to remove residual reagents and subsequently with chloroform. The chloroform fraction was evaporated to dryness, redissolved in minimum amount hot toluene and precipitated into methanol (100 mL of methanol and 0.5 mL of concentrated HCl). After drying in vacuum the product was obtained as a dark olive green solid.

Yield: 0.09 g (90%). M_n = 7.2 kDa, M_w = 13.7 kDa, polydispersity index (*PDI*) = 1.90. ^{1}H NMR (400 MHz, $CDCl_3$): δ = 8.43 (2H, s, H_{vinyl}), 6.98 (56H, s, H_{ar}), 2.81 (112H, t, α-CH_2), 1.77−1.65 (112H, m, β-CH_2), 1.49−1.27 (336H, m, CH_2), 0.95−0.84 (168H, m, CH_3).

■ ASSOCIATED CONTENT

Supporting Information. ^{1}H NMR spectra of **OHC-P1-CHO** and **P3** in chloroform; UV−vis absorption spectra of **P1** in chloroform solutions and solid-state on glass; CVs of **P1** to **P3** as drop cast films on a glassy carbon electrode; IR-spectra of **P1**-**P3**; TGA traces of **P1**−**P3** under nitrogen; DSC traces of **P1**−**P3** under nitrogen; Photographs of solutions of **P1**, **P2**, and **P3**; EIS spectra of **P1**. This material is available free of charge via the Internet at http://pubs.acs.org.

■ AUTHOR INFORMATION

Corresponding Author

*E-mail: thomas.baumgartner@ucalgary.ca (T.B.); todd.sutherland@ucalgary.ca (T.S.).

■ ACKNOWLEDGMENT

We thank NSERC of Canada, Canada School of Energy and Environment, Canadian Foundation for Innovation, Alberta Small Equipment Grants Program, and the Berlinguette lab for use of the DSSC assembling and testing equipment. T.B. thanks Alberta Ingenuity—now part of Alberta Innovates Technology Futures—for a New Faculty Award.

■ REFERENCES

(1) (a) Hagfeldt, A.; Boschloo, G.; Sun, L.; Kloo, L.; Pettersson, H. *Chem. Rev.* **2010**, *110*, 6595–6663. (b) O'Regan, B.; Grätzel, M. *Nature* **1991**, *353*, 737–740.

(2) (a) Thompson, B. C.; Fréchet, J. M. J. *Angew. Chem., Int. Ed.* **2008**, *47*, 58–77. (b) Cheng, Y.-J.; Yang, S.-H.; Hsu, C.-S. *Chem. Rev.* **2009**, *109*, 5868–5923. (c) Beaujuge, P. M.; Amb, C. M.; Reynolds, J. R. *Acc. Chem. Res.* **2010**, *43*, 1396–1407. (d) Helgesen, M.; Sondergaard, R.; Krebs, F. C. *J. Mater. Chem.* **2010**, *20*, 36–60.

(3) (a) Yu, Q.; Wang, Y.; Yi, Z.; Zu, N.; Zhang, J.; Zhang, M.; Wang, P. *ACS Nano* **2010**, *4*, 6032–6038. (b) Chen, C.-Y.; Wang, M.; Li, J.-Y.; Pootrakulchote, N.; Alibabaei, L.; Ngoc-le, C.-h.; Decoppet, J.-D.; Tsai, J.-H.; Grätzel, C.; Wu, C.-G.; Zakeeruddin, S. M.; Grätzel, M. *ACS Nano* **2009**, *3*, 3103–3109.

(4) (a) Zeng, W.; Cao, Y.; Bai, Y.; Wang, Y.; Shi, Y.; Zhang, M.; Wang, F.; Pan, C.; Wang, P. *Chem. Mater.* **2010**, *22*, 1915–1925. (b) Caballero, R. n.; Barea, E. M.; Fabregat-Santiago, F.; de la Cruz, P.; Márquez, L.; Langa, F.; Bisquert, J. *J. Phys. Chem. C* **2008**, *112*, 18623 18627.

(5) (a) Hou, J.; Chen, H.-Y.; Zhang, S.; Chen, R. I.; Yang, Y.; Wu, Y.; Li, G. *J. Am. Chem. Soc.* **2009**, *131*, 15586–15587. (b) Liang, Y.; Xu, Z.; Xia, J.; Tsai, S.-T.; Wu, Y.; Li, G.; Ray, C.; Yu, L. *Adv. Mater.* **2010**, *22*, E135–E138.

(6) Ma, W.; Yang, C.; Gong, X.; Lee, K.; Heeger, A. J. *Adv. Funct. Mater.* **2005**, *15*, 1617–1622.

(7) (a) Liu, Y.; Summers, M. A.; Edder, C.; Fréchet, J. M. J.; McGehee, M. D. *Adv. Mater.* **2005**, *17*, 2960–2964. (b) Liu, X.; Zhu, R.; Zhang, Y.; Liu, B.; Ramakrishna, S. *Chem. Commun.* **2008**, 3789 3791. (c) Lohwasser, R. H.; Bandara, J.; Thelakkat, M. *J. Mater. Chem.* **2009**, *19*, 4126–4130. (d) Fang, Z.; Eshbaugh, A. A.; Schanze, K. S. *J. Am. Chem. Soc.* **2011**, *133*, 3063–3069. (e) Wang, M.; Wang, X. *Sol. Energy Mater. Sol. Cells* **2007**, *91*, 1782–1787. (f) Liu, Y.; Scully, S. R.; McGehee, M. D.; Liu, J.; Luscombe, C. K.; Fréchet, J. M. J.; Shaheen, S. E.; Ginley, D. S. *J. Phys. Chem. B* **2006**, *110*, 3257–3261. (g) Kim, Y.-G.; Walker, J.; Samuelson, L. A.; Kumar, J. *Nano Lett.* **2003**, *3*, 523–525. (h) Senadeera, G. K. R.; Nakamura, K.; Kitamura, T.; Wada, Y.; Yanagida, S. *Appl. Phys. Lett.* **2003**, *83*, 5470–5472. (i) Mwaura, J. K.; Zhao, X.; Jiang, H.; Schanze, K. S.; Reynolds, J. R. *Chem. Mater.* **2006**, *18*, 6109–6111. (j) Senadeera, G. K. R.; Kitamura, T.; Wada, Y.; Yanagida, S. *Sol. Energy Mater. Sol. Cells* **2005**, *88*, 315–322. (k) Coakley, K. M.; McGehee, M. D. *Appl. Phys. Lett.* **2003**, *83*, 3380–3382. (l) Zhang, W.; Fang, Z.; Su, M.; Saeys, M.; Liu, B. *Macromol. Rapid Commun.* **2009**, *30*, 1533–1537. (m) Liu, J.; Kadnikova, E. N.; Liu, Y.; McGehee, M. D.; Fréchet, J. M. J. *J. Am. Chem. Soc.* **2004**, *126*, 9486–9487.

(8) (a) An, B.-K.; Hu, W.; Burn, P. L.; Meredith, P. *J. Phys. Chem. C* **2010**, *114*, 17964–17974. (b) Mosurkal, R.; He, J.-A.; Yang, K.; Samuelson, L. A.; Kumar, J. *J. Photochem. Photobiol., A* **2004**, *168*, 191 196. (c) Rice, C. R.; Ward, M. D.; Nazeeruddin, M. K.; Grätzel, M. *New J. Chem.* **2000**, *24*, 651–652.

(9) Wang, Z.-S.; Li, F.-Y.; Huang, C.-H. *Chem. Commun.* **2000**, 20632064.

(10) Brennan, B. J.; Keirstead, A. E.; Liddell, P. A.; Vail, S. A.; Moore, T. A.; Moore, A. L.; Gust, D. *Nanotechnology* **2009**, *20*, 505203.

(11) (a) Park, H.; Bae, E.; Lee, J.-J.; Park, J.; Choi, W. *J. Phys. Chem. B* **2006**, *110*, 8740–8749. (b) Pechy, P.; Rotzinger, F. P.; Nazeeruddin, M. K.; Kohle, O.; Zakeeruddin, S. M.; Humphry-Baker, R.; Gräetzel, M. *J. Chem. Soc., Chem. Commun.* **1995**, 65–66.

(12) Krebs, F. C.; Senkovskyy, V.; Kiriy, A. *IEEE J. Sel. Top. Quantum Electron.* **2010**, *16*, 1821–1826.

(13) (a) Jiang, H.; Zhao, X.; Shelton, A. H.; Lee, S. H.; Reynolds, J. R.; Schanze, K. S. *ACS Appl. Mater. Interfaces* **2009**, *1*, 381–387. (b) Yanagida, S.; Senadeera, G. K. R.; Nakamura, K.; Kitamura, T.; Wada, Y. *J. Photochem. Photobiol., A* **2004**, *166*, 75–80.

(14) Loewe, R. S.; Khersonsky, S. M.; McCullough, R. D. *Adv. Mater.* **1999**, *11*, 250–253.

(15) (a) Iovu, M. C.; Sheina, E. E.; Gil, R. R.; McCullough, R. D. *Macromolecules* **2005**, *38*, 8649–8656. (b) Lohwasser, R. H.; Thelakkat, M. *Macromolecules* **2011**, *44*, 3388–339710.1021/ma200119s.

(16) Mishra, A.; Fischer, M. K. R.; Bäuerle, P. *Angew. Chem., Int. Ed.* **2009**, *48*, 2474–2499.
(17) (a) Jeffries-EL, M.; Sauvé, G.; McCullough, R. D. *Adv. Mater.* **2004**, *16*, 1017–1019. (b) Jeffries-EL, M.; Sauvé, G.; McCullough, R. D. *Macromolecules* **2005**, *38*, 10346–10352. (c) Liu, J.; McCullough, R. D. *Macromolecules* **2002**, *35*, 9882–9889.
(18) McCullough, R. D. *Adv. Mater.* **1998**, *10*, 93–116.
(19) Surin, M.; Coulembier, O.; Tran, K.; Winter, J. D.; Leclère, P.; Gerbaux, P.; Lazzaroni, R.; Dubois, P. *Org. Electron* **2010**, *11*, 767–774.
(20) Li, Y.; Cao, Y.; Gao, J.; Wang, D.; Yu, G.; Heeger, A. J. *Synth. Met.* **1999**, *99*, 243–248.
(21) Satapathi, S.; Yan, F.; Anandakathir, R.; Yang, K.; Li, L.; Mosurkal, R.; Samuelson, L. A.; Kumar, J. *J. Macromol. Sci., Part A: Pure Appl. Chem.* **2010**, *47*, 1180–1183.
(22) Xu, W.; Pei, J.; Shi, J.; Peng, S.; Chen, J. *J. Power Sources* **2008**, *183*, 792–798.
(23) Chen, T.-A.; Wu, X.; Rieke, R. D. *J. Am. Chem. Soc.* **1995**, *117*, 233–244.
(24) Holdcroft, S. *J. Polym. Sci., Part B: Polym. Phys.* **1991**, *29*, 1585–1588.